Journal Pre-proof

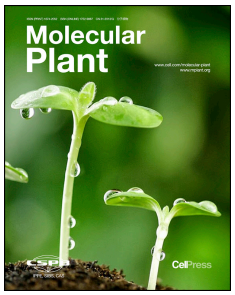

Regulation of the Stability and ABA Import Activity of NRT1.2/NPF4.6 by CEPR2-mediated Phosphorylation in *Arabidopsis*

Lei Zhang, Zipeng Yu, Yang Xu, Miao Yu, Yue Ren, Shizhong Zhang, Guodong Yang, Jinguang Huang, Kang Yan, Chengchao Zheng, Changai Wu

PII: S1674-2052(21)00009-5
DOI: https://doi.org/10.1016/j.molp.2021.01.009
Reference: MOLP 1079

To appear in: *MOLECULAR PLANT*
Accepted Date: 11 January 2021

Please cite this article as: **Zhang L., Yu Z., Xu Y., Yu M., Ren Y., Zhang S., Yang G., Huang J., Yan K., Zheng C., and Wu C.** (2021). Regulation of the Stability and ABA Import Activity of NRT1.2/NPF4.6 by CEPR2-mediated Phosphorylation in *Arabidopsis*. Mol. Plant. doi: https://doi.org/10.1016/j.molp.2021.01.009.

Regulation of the Stability and ABA Import Activity of NRT1.2/NPF4.6 by CEPR2-mediated Phosphorylation in *Arabidopsis*

Lei Zhang[1, δ], Zipeng Yu[1, δ], Yang Xu[1], Miao Yu[2], Yue Ren[1], Shizhong Zhang[1], Guodong Yang[1], Jinguang Huang[1], Kang Yan[1], Chengchao Zheng[1, *] and Changai Wu[1, *]

[δ] These authors contributed equally to this work.

[1] State Key Laboratory of Crop Biology, Shandong Engineering Research Center of Plant-Microbial Restoration for Saline-Alkali Land, College of Life Sciences, Shandong Agricultural University, Tai'an 271018, China

[2] State Key Laboratory of Plant Physiology and Biochemistry, College of Biological Sciences, China Agricultural University, Beijing 100193, China

*** Corresponding authors**

Chengchao Zheng: cczheng@sdau.edu.cn; Tel: 86-538-8242894

Changai Wu: cawu@sdau.edu.cn; Tel: 86-538-8246858

Short Summary

NRT1.2/NPF4.6, as an ABA transporter, is phosphorylated by CEPR2 in the absence of ABA and subsequently degraded by UBC32/33/34. However, ABA inhibits CEPR2-mediated phosphorylation of NRT1.2/NFP4.6, and the ABA import activity and protein stability of NRT1.2/NPF4.6 are significantly restored, thus initiating plant stress response.

E-mails:

Lei Zhang: zhanganqi2002@163.com

Zipeng Yu: yzp52120090916@163.com

Yang Xu: xy52120092661@163.com

Miao Yu: ym15600911706@126.com

Yue Ren: renyue1997@163.com

Shizhong Zhang: shizhong@sdau.edu.cn

Guodong Yang: gdyang@sdau.edu.cn

Jinguang Huang: jghuang@sdau.edu.cn

Kang Yan: kangyan@sdau.edu.cn

Chengchao Zheng: cczheng@sdau.edu.cn

Changai Wu: cawu@sdau.edu.cn

Abstract

Abscisic acid (ABA) transport plays an important role in systemic plant responses to environmental factors. In this study, we showed that C-terminally encoded peptide receptor 2 (CEPR2) directly interacts with the ABA transporter NRT1.2/NPF4.6. Using transgenic seedlings, we demonstrated that NRT1.2/NPF4.6 positively regulated the ABA response, and that NRT1.2/NPF4.6 was epistatically and negatively regulated by CEPR2. Under normal conditions, CEPR2 phosphorylated NRT1.2/NPF4.6 at serine 292 to promote its degradation. However, ABA treatment and non-phosphorylation at serine 292 prevented degradation of NRT1.2/NPF4.6, indicating that ABA inhibits phosphorylation of this residue. Transport assays in yeast and *Xenopus* oocytes revealed that non-phosphorylated NRT1.2/NPF4.6 had high levels of ABA import activity, whereas phosphorylated NRT1.2/NPF4.6 did not import ABA. Analyses of complemented *nrt1.2* mutants that mimicked non-phosphorylated and phosphorylated NRT1.2/NPF4.6 confirmed that non-phosphorylated NRT1.2^{S292A} had high stability and ABA import activity *in planta.* Additional experiments showed that NRT1.2/NPF4.6 was degraded via the 26S proteasome and vacuolar degradation pathways. UBC32, UBC33, and UBC34 interacted with NRT1.2/NPF4.6 in the endoplasmic reticulum and mediated its ubiquitination. NRT1.2/NPF4.6 is epistatically and negatively regulated by UBC32, UBC33, and UBC34 *in planta*. Taken together, these results suggested that the stability and ABA import activity of NRT1.2/NPF4.6 are precisely regulated by its phosphorylation and degradation in response to environmental stress.

Keywords

CEPR2; NRT1.2/NPF4.6; phosphorylation; UBC32, UBC33, and UBC34; degradation; import activity

Introduction

Plants must continuously adapt to adverse environmental conditions, including temperature, salinity, and drought (Li et al., 2019; Soma et al., 2017; Teardo et al., 2019; Xu et al., 2018; Yang et al., 2019; Zhang et al., 2018). Upon sensing environmental stressors, plants stop growing and trigger protective responses (Wang et al., 2018; Yu et al., 2020). Once environmental stress subsides, plants quickly deactivate these protective responses and reinitiate growth (Wang et al., 2018). Thus, rapid responses to adverse conditions are critical for plant growth and survival, but the mechanisms underlying these responses are not fully understood.

Abscisic acid (ABA), a stress hormone, plays critical roles in the regulation of both plant growth and multiple stress responses (Cutler et al., 2010; Raghavendra et al., 2010). In response to environmental stress, ABA accumulates rapidly and is transported from the site of synthesis to the site of action, where it is recognized by ABA receptors of the pyrabactin resistance 1 family (PYR1); these proteins are also referred to as PYR1-like (PYL) (Boursiac et al., 2013). ABA is predominantly produced in vascular tissues in response to drought stress (Boursiac et al., 2013). Therefore, ABA signaling

in plants relies on the export of ABA from the cells that synthesize it as well as the import of ABA into target cells (Kuromori et al., 2018). Several ABA transporters have been identified, including two *Arabidopsis* AT-binding cassette (ABC) transporters, ABCG25 and ABCG40 (Kang et al., 2015; Kuromori et al., 2010). Loss-of-function studies revealed that both proteins are associated with ABA sensitivity and stomatal closure (Kang et al., 2015; Kuromori et al., 2010). Additional biochemical characterization studies using heterologous expression systems have shown that ABCG25, ABCG30, ABCG31, and ABCG40 exhibit ABA export or import activity. AtDTX50, a member of the multidrug and toxin efflux (MATE) transporter family (Zakrzewska et al., 2019), has also been identified as an ABA exporter (Zhang et al., 2014). Finally, functional screening in a yeast system identified NPF4.6, an *Arabidopsis* NITRATE TRANSPORTER 1/PEPTIDE TRANSPORTER FAMILY (NPF) member, that mediates the cellular uptake of ABA; the protein was subsequently renamed AIT1 (Kanno et al., 2012; Leran et al., 2020). Because NPF4.6 was previously identified as the low-affinity nitrate transporter NRT1.2/NPF4.6 (Huang et al., 1999), we use that designation herein. The mechanisms underlying ABA transporter function, particularly with respect to posttranslational regulation, have not been extensively explored.

Previously, we reported that CEPR2, a typical leucine-rich repeat receptor-like kinase (LRR-RLK), controls the ABA response in *Arabidopsis* by regulating the phosphorylation and degradation of ABA-receptor PYLs (Yu et al., 2019). These findings demonstrated, for the first time, that a plasma-membrane-localized LRR-RLK regulates ABA receptors. However, a thorough understanding of the mechanisms underlying the CEPR2-mediated ABA response is lacking. Hence, in this study, we sought to determine whether CEPR2 regulates ABA transporters. We found that the CEPR2-mediated ABA response is activated by ABA-mediated inhibition of NRT1.2/NPF4.6 phosphorylation at serine 292 (Ser^{292}). Thus, we identified a novel target of CEPR2 and elucidated the regulatory mechanisms underlying ABA transporter activity and the stability of NRT1.2/NPF4.6.

Results

The loop region of NRT1.2/NPF4.6 interacts with the kinase domain of CEPR2

To identify new targets of CEPR2 in response to ABA, we compared the phosphoproteomes (Supplementary Fig. 1A) of wild-type (WT) *Arabidopsis* seedlings to those of *CEPR2-OE-9* seedlings; *CEPR2-OE-9* is a previously developed *Arabidopsis* line that overexpresses *CEPR2* (Yu et al., 2019). Between the two genotypes, we identified 169 differentially regulated phosphopeptides ($P \leq 0.05$ and fold-change ≥ 1.20 or ≤ 0.8); 97 peptides belonging to 78 proteins were upregulated, and 72 peptides belonging to 68 proteins were downregulated (Supplementary Excel 1). To identify the directly phosphorylated target proteins of CEPR2, we investigated whether the 78 proteins whose phosphorylation was upregulated (Supplementary Table 1) interacted with CEPR2. To this end, we performed yeast two-hybrid (Y2H)

experiments with the mating-based split ubiquitin system (MbSUS) (Supplementary Fig. 1). Ten of the proteins interacted with CEPR2. Of those, NRT1.2/NPF4.6 (protein number 46) was previously identified as the ABA importer AIT1 (Huang et al., 1999; Kanno et al., 2012). Therefore, we selected NRT1.2/NPF4.6 for further analysis.

To confirm the interaction between NRT1.2/NPF4.6 and CEPR2, we performed firefly luciferase complementation imaging (LCI) assays in *Nicotiana benthamiana* leaves. The results were consistent with the MbSUS results showing that NRT1.2/NPF4.6 interacted with CEPR2 (Fig. 1A). Next, we transiently co-expressed split YFP combinations (CEPR2-YFP^N and NRT1.2-YFP^C) in *N. benthamiana* leaves. Bimolecular fluorescence complementation (BiFC) assays, in conjunction with N-(3-triethylammomiumpropyl) 4-(p-diethylaminophenylhexatrienyl) (FM4-64) staining, showed that NRT1.2/NPF4.6 and CEPR2 interacted at the plasma membrane (Fig. 1B). Differential phosphoproteome analysis revealed that the phosphorylation sites of NRT1.2/NPF4.6 were serine residues 277 and 292 (Ser^{277} and Ser^{292}) (Supplementary Excel 1). These two sites are located in the cytosolic loop region of NRT1.2/NPF4.6 between of the 12 transmembrane regions (Fig. 1C). To further examine the interaction between NRT1.2/NPF4.6 and CEPR2, we performed pull-down assays using the cytosolic loop region of NRT1.2/NPF4.6 ($NRT1.2^{loop}$) and a series of CEPR2 deletion constructs developed previously (Yu et al., 2019). The results indicated that the $NRT1.2^{loop}$ interacted with the kinase domain of CEPR2 ($CEPR2^{KD}$) (Fig. 1D). Next, we expressed $NRT1.2^{loop}$-GST and $CEPR2^{KD}$-His in *Escherichia coli* and purified the recombinant proteins. Pull-down assays confirmed that $NRT1.2^{loop}$ interacted with $CEPR2^{KD}$ (Fig. 1E). The expression levels of genes encoding ABA transporters did not differ significantly among *CEPR2-OE-9*, WT, and *cepr2-1* seedlings grown on 1/2 MS with or without 1 μM ABA (*cepr2-1* seedlings were developed previously in (Yu et al., 2019); Supplementary Fig. 2). Of the proteins encoded by these genes, only NRT1.2/NPF4.6 interacted with CEPR2 (Fig. 1F). Together, these experiments demonstrated that the NRT1.2/NPF4.6 loop region interacts with the CEPR2 kinase domain both *in vitro* and in plant cells.

NRT1.2/NPF4.6 positively regulates the ABA-mediated inhibition of seed germination and primary root growth

To assess the role of NRT1.2/NPF4.6 in the ABA response, we used two independent *Arabidopsis* lines overexpressing *NRT1.2/NPF4.6* (*NRT1.2-OE-1* and *NRT1.2-OE-2*) (Fig. 2A) and two T-DNA insertion mutants of *NRT1.2/NPF4.6* (*nrt1.2-1* and *nrt1.2-2*) (Fig. 2B). Reverse transcription-polymerase chain reaction (RT-PCR) and western blotting demonstrated that NRT1.2/NPF4.6 was overexpressed in transgenic *NRT1.2-OE-1* and *NRT1.2-OE-2* plants. Although the expression levels of NRT1.2/NPF4.6 in *nrt1.2-2* seedlings were similar to those in WT seedlings, NRT1.2/NPF4.6 protein levels were substantially lower in the two mutants than in WT seedlings (Fig. 2C). Under normal conditions, the *NRT1.2-OE* and *nrt1.2* plants exhibited primary root growth and seed germination rates similar to those of WT (Fig. 2D, E and F). However, when treated with ABA, the *NRT1.2-OE* plants had shorter primary roots and lower seed germination

rates than WT plants. By contrast, ABA-treated *nrt1.2* mutant plants developed more quickly and had longer primary roots (Fig. 2D-F). These results suggested that NRT1.2/NPF4.6 positively regulates the ABA response.

CEPR2 phosphorylates NRT1.2/NPF4.6 at Ser^{292}, playing a vital role in maintaining NRT1.2/NPF4.6 stability

Next, to investigate the effects of CEPR2 on NRT1.2/NPF4.6, we performed a genetic phenotype analysis. The results showed that the root length and seed germination rate of the *cepr2-1nrt1.2-1* double mutant were similar to those of the *nrt1.2-1* single mutant, but greater than those of the *cepr2-1* mutant (Fig. 2D-F). This genetic evidence, in conjunction with the observation that CEPR2 and NRT1.2/NPF4.6 interacted, suggested that negatively regulates NRT1.2/NPF4.6, possibly by influencing its stability or import activity. To test this possibility, we performed cell-free degradation assays using NRT1.2^{loop}-GST with protein extracts from *CEPR2-OE-9*, WT, and *cepr2-1* seedlings. Under normal conditions, 53%, 68%, and 12% of the NRT1.2^{loop}-GST remained after a 60-min incubation with protein extracts from WT, *cepr2-1*, and *CEPR2-OE-9* seedlings, respectively (Fig. 3A, B), indicating that CEPR2 promotes the degradation of NRT1.2/NPF4.6 under normal conditions. By contrast, in the presence of ABA, 63%, 80%, and 48% of the NRT1.2^{loop}-GST remained after a 60 min incubation with protein extracts from WT, *cepr2-1*, and *CEPR2-OE-9* seedlings, respectively (Fig. 3A, B), indicating that ABA prevents the CEPR2-mediated degradation of NRT1.2^{loop}-GST.

Phosphorylation regulates protein stability, protein activity, interaction, and subcellular localization (Chen et al., 2018). Hence, we hypothesized that the effects of CEPR2 on NRT1.2/NPF4.6 stability might be regulated by the phosphorylation states of Ser^{277} or Ser^{292}. To test this idea, we generated variants of NRT1.2/NPF4.6 in which Ser^{277}or Ser^{292} were mutated to similarly sized amino acids: neutral alanine (A), which is non-phosphorylatable, and negatively charged aspartate (D), which mimics a constitutively phosphorylated state. Both single and double mutants were constructed: NRT1.2^{loopS277A}, NRT1.2^{loopS292A}, NRT1.2^{loopS277D}, NRT1.2^{loopS292D}, NRT1.2^{loopS277AS292A}, and NRT1.2^{loopS277DS292D} (Supplementary Fig. 3, 4A). The mutations at Ser^{277} or Ser^{292} did not affect the interaction between NRT1.2/NPF4.6 and CEPR2. Next, we purified CEPR2-GFP fusion proteins from transgenic seedlings obtained previously (Yu et al., 2019). NRT1.2^{loop} proteins codon-optimized for *E. coli* were used to perform *in vitro* kinase assays. When CEPR2-GFP was incubated with NRT1.2^{loop}-GST in kinase buffer, phosphorylation of NRT1.2^{loop}-GST increased (Fig. 3C). As expected, treatment with calf intestinal alkaline phosphatase (CIAP) decreased the phosphorylation of NRT1.2^{loop}-GST. Together, these observations suggested that NRT1.2^{loop}-GST is phosphorylated by CEPR2.

We then incubated CEPR2-GFP with NRT1.2/NPF4.6 mutated at Ser^{277} and/or Ser^{292}. Subsequent *in vitro* kinase assays revealed that after 2 h, the phosphorylation level of NRT1.2^{loopS277A}-GST was similar to that of NRT1.2^{loop}-GST. However, no phosphorylation was detected in NRT1.2^{loopS292A}-GST (Fig. 3C, D). These data indicated that Ser^{292}, but not Ser^{277}, is the target of phosphorylation by CEPR2.

Next, we compared the degradation of NRT1.2^{loopS292A} to that of NRT1.2^{loop}. Degradation of NRT1.2^{loopS292A} was significantly reduced relative to NRT1.2^{loop}, irrespective of ABA treatment (Fig. 3E, F). Specifically, the level of NRT1.2^{loopS292A} in the absence of ABA was similar to the level of NRT1.2^{loop} in the presence of ABA. These observations suggested that Ser^{292} plays a vital role in the phosphorylation-dependent degradation of NRT1.2/NPF4.6.

NRT1.2/NPF4.6 phosphorylation eliminates NRT1.2/NPF4.6-mediated ABA import

We further investigated the effect of NRT1.2/NPF4.6 non-phosphorylation on ABA import activity. Using a Y2H method described previously (Kanno et al., 2012), yeast cells were co-transformed with AD-ABI1 (ABI1 fused to the GAL4 activation domain) and BD-PYR1 (PYR1 fused to the GAL4 DNA-binding domain). These co-transformed cells were further transformed by pYES2 containing NRT1.2 or series of NRT1.2 mutant at Ser^{277} or Ser^{292}. Relative to pYES2-transformed yeast cells, pYES2-NRT1.2-transformed yeast cells grew better in the presence of 1 μM ABA (Supplementary Fig. 4B). However, no obvious growth differences were observed between pYES2 and pYES2-NRT1.2 yeast cells in the presence of 4 μM ABA, indicating that it was necessary to determine the optimal ABA concentration for subsequent experiments.

None of the transformed yeast cells grew in -WLUAH media. However, in the presence of 1 μM ABA, yeast cells transformed with non-phosphomimic forms of NRT1.2/NPF4.6, such as pYES2-NRT1.2^{S277A}, pYES2-NRT1.2^{S292A}, and pYES2-NRT1.2^{S277AS292A}, or with the Ser^{277} phosphomimic form (pYES2-NRT1.2^{S277D}), had high growth rates similar to those of yeast cells transformed with pYES2-NRT1.2. By contrast, yeast cells transformed with Ser^{292} phosphomimic forms (pYES2-NRT1.2^{S292D} and pYES2-NRT1.2^{S277DS292D}) had low growth rates similar to that of pYES2-NRT1.2+CEPR2 (Fig. 4A, Supplementary Fig. 4C). These results suggested that NRT1.2/NPF4.6 not phosphorylated at Ser^{292} (NRT1.2^{S292A}) exhibits ABA import activity in yeast cells, and that CEPR2 inhibits the ABA-import activity of NRT1.2/NPF4.6, possibly via phosphorylation at Ser^{292}.

We then compared ABA import activity in *Xenopus* oocytes by measuring ABA content. *Xenopus* oocytes expressing NRT1.2 and NRT1.2^{S292A} had similar levels of ABA, which were significantly higher than those of negative control *Xenopus* oocytes injected with water (Fig. 4B). The levels of ABA in *Xenopus* oocytes expressing NRT1.2^{S292D}, CEPR2, NRT1.2^{S292D}+CEPR2 or CEPR2+NRT1.2 did not differ significantly from those in the negative control (Fig. 4B, Supplementary Fig. 4D). At the same time, the levels of ABA in *Xenopus* oocytes expressing AIT3, another ABA transporter characterized by Kanno et al. (2012), was also higher from those in the negative control (Supplementary Fig. 4D). These results provided further confirmation that NRT1.2^{S292A}, but not NRT1.2^{S292D}, imported ABA, and that CEPR2 mediated the phosphorylation of NRT1.2/NPF4.6 at Ser^{292} in *Xenopus* oocytes.

NRT1.2, NRT1.2^{S292A}, and NRT1.2^{S292D} were separately introduced into *nrt1.2-1* mutants to obtain complemented plants (designated *NRT1.2-COMs*, *NRT1.2^{S292A}-COMs* and *NRT1.2^{S292D}-COMs*, respectively). The genotypes of these plants were verified by RT-PCR (Supplementary Fig. 5A). In the absence of ABA, the growth rates and phenotypes of all transgenic plants, irrespective of genotype, were similar to those of WT (Fig. 4C). When exposed to ABA, the root growth of *NRT1.2-COM* plants was similar to that of WT, i.e., both the high root growth of the *nrt1.2-1* plants and the low root growth of *NRT1.2-OE-1* plants were rescued. The root growth of *NRT1.2^{S292A}-COM* plants was similar to that of *NRT1.2-OE-1* plants, whereas the root growth of *NRT1.2^{S292D}-COM* plants was similar to that of *nrt1.2-1* plants (Fig. 4C and D). NRT1.2/NPF4.6 protein levels in the *NRT1.2^{S292A}-COM* plants were higher than those in WT and similar to those in *NRT1.2-COM* plants, i.e., NRT1.2/NPF4.6 protein levels in *NRT1.2^{S292A}-COM* and *NRT1.2-COM* plants were higher than those in WT. By contrast, NRT1.2/NPF4.6 protein levels in NRT1.2^{S292D}-COM plants were similar to those in *nrt1.2-1* plants (Fig. 4E). Furthermore, ABA levels in *NRT1.2^{S292A}-COM* and *NRT1.2-OE-1* plants were higher than those in the WT, whereas ABA levels in the *NRT1.2^{S292D}-COM* plants and the *nrt1.2-1* plants were lower than those in WT (Fig. 5F). These results indicated that NRT1.2^{S292A} is stable and effectively imports ABA *in planta*.

UBC32, UBC33, and UBC34 mediate the degradation of NRT1.2/NPF4.6

To further investigate the NRT1.2/NPF4.6 degradation pathway, we treated protein extracts from 7-day-old *CEPR2-OE-9* seedlings with 50 μM MG132 (an inhibitor of the 26S proteasome degradation pathway), 50 μM E64d (an inhibitor of the vacuolar degradation pathway), or both compounds prior to incubation with purified NRT1.2^{loop}-GST. After incubation, NRT1.2/NPF4.6 degradation was significantly inhibited by MG132 or E64d, but not by dimethyl sulfoxide (DMSO, the vehicle control; Fig. 5A). For example, after a 2-h incubation of NRT1.2^{loop}-GST with protein extracts from 7-day-old *CEPR2-OE-9* seedlings treated with DMSO, 11% of the NRT1.2^{loop}-GST remained; by contrast, after a 2-h incubation of NRT1.2^{loop}-GST with protein extracts from 7-day-old *CEPR2-OE-9* seedlings treated with MG132, E64d, or both, 58%, 80%, and 99%, respectively, of the NRT1.2^{loop}-GST remained (Fig. 5B). These observations suggested that NRT1.2/NPF4.6 degradation is mediated by both the 26S proteasome and vacuolar degradation pathways. In addition, despite of the presence of ABA or MG132 and E64d, NRT1.2-GFP was observed on both plasma membrane (PM) and endoplasmic reticulum (ER), NRT1.2^{S292A}-GFP was observed on the PM, whereas NRT1.2^{S292A}-GFP and NRT1.2^{S292D}-GFP was observed on PM or ER membrane only under overexposure conditions (Supplementary Figure 6), indicating that the phosphorylation of NRT1.2 changed its localization from PM to ER membrane to degradation.

To identify the components that mediate the degradation of NRT1.2/NPF4.6, we searched the BioGRID web site (https://thebiogrid.org/) and found UBIQUITIN-CONJUGATING ENZYME 34 (UBC34) among the interacting proteins (Xu et al., 2020). UBC34, which is an E2 ligase with ubiquitination activity, is highly similar to UBC32 and UBC33 (Cui et

al., 2012a; Cui et al., 2012b). NRT1.2/NPF4.6 interacted with UBC32, UBC33, and UBC34 in yeast (Fig. 5C). Pull-down assays using NRT1.2/NPF4.6 and UBC mutants lacking the transmembrane region (Supplementary Fig. 7) further confirmed the interactions between NRT1.2^{loop} and each of the three UBCs (Fig. 5D). Moreover, BiFC assays, in conjunction with ER-tracker in the presence of MG132 and E64d, showed that NRT1.2/NPF4.6 and UBC32, UBC33, and UBC34 interacted on the ER (Fig. 5E).

Next, we investigated the UBC-mediated ubiquitination of NRT1.2/NPF4.6 in greater detail. *In vitro* ubiquitination analysis indicated that UBC32, UBC33, and UBC34 self-ubiquitinated (Fig. 5F), confirming that these UBCs possess ubiquitination activity. However, when point-mutated forms of UBC32 (C93S), UBC33 (C87S), or UBC34 (C87S) were used, neither ubiquitin nor ubiquitination were detected (Fig. 5F), suggesting that Cys93 (in UBC32) and Cys87 (in UBC33 and UBC34) play important roles in ubiquitination. Next, we investigated the UBC-dependent ubiquitination of NRT1.2/NPF4.6 using a semi-*in vitro* assay in which protein extracts from a triple mutant of UBC32, UBC33, and UBC34 (*ubc323334*) overexpressing NRT1.2/NPF4.6 were incubated with purified UBC32$^{\Delta TM}$-His, UBC33$^{\Delta TM}$-His, or UBC34$^{\Delta TM}$-His. Ubiquitinated NRT1.2/NPF4.6 was only detected in the presence of UBC32, UBC33, or UBC34 (Fig. 5G), suggesting that UBC32, UBC33, and UBC34 can each mediate ubiquitination of NRT1.2/NPF4.6.

Finally, we generated *NRT1.2-OE-1/ubc323334* and *nrt1.2ubc323334* mutant plants by overexpressing NRT1.2/NPF4.6 in *ubc323334* and crossing *nrt1.2* with *ubc323334*, respectively. The genotypes of the resultant plants were confirmed using RT-PCR (Supplementary Fig. 5B, C). Genetic analysis showed that during seed germination, the *NRT1.2-OE-1/ubc323334* plants had phenotypes similar to those of the *ubc323334* and *NRT1.2-OE-1* plants. All transgenic plants were more sensitive to ABA than the WT plants. By contrast, the *nrt1.2ubc323334* mutant had a phenotype similar to that of *nrt1.2-1* mutant and was less sensitive to ABA than the WT (Fig. 6A, B). When exposed to ABA, the root lengths of *NRT1.2-OE-1/ubc323334*, *ubc323334*, and *NRT1.2-OE-1* plants were similar to each other and shorter than those of WT; the root lengths of *nrt1.2ubc323334* and *nrt1.2-1* mutants were also similar to each other and longer than those of WT (Fig. 6C, D). Under normal conditions, NRT1.2/NPF4.6 protein content was much higher in *ubc323334* than in WT plants. However, in the presence of ABA, NRT1.2/NPF4.6 protein content in the *ubc323334* mutant was similar to that in WT plants (Fig. 6E, F). These results indicated that NRT1.2/NPF4.6 is epistatically and negatively regulated by UBC32, UBC33, and UBC34 via ubiquitination modification.

Discussion

ABA transporters play critical roles in the systemic ABA response in plants (Kuromori et al., 2018). Although several ABA transporters have been identified (Huang et al., 1999; Kang et al., 2015; Kanno et al., 2012; Kuromori et al., 2010; Zhang et al., 2014), the mechanisms that regulate ABA transporters remain largely unknown. Our identification of CEPR2,

UBC32, UBC33, and UBC34 as regulators of NRT1.2/NPF4.6 helps to clarify the molecular mechanisms that modulate ABA import.

CEPR2 was originally characterized by Tabata et al. (2014) as one of two receptors of C-TERMINALLY ENCODED PEPTIDE (CEP). Although CEPR2 plays minor roles in response to nitrogen starvation in *Arabidopsis* (Tabata et al., 2014), we found previously that CEPR2, but not CEPR1, interacts with and phosphorylates PYL4 to promote its degradation under normal conditions (Yu et al., 2019). However, CEPR2 cannot phosphorylate PYL4 in the presence of ABA (Yu et al., 2019), indicating that CEPR2 plays a regulatory role in the ABA response and plant growth. In this study, to identify new targets of CEPR2 in response to ABA, we compared the phosphoproteomes of CEPR2-overexpressing and WT seedlings. In seedlings overexpressing CEPR2, phosphorylation of NRT1.2/NPF4.6 at S292 and S277 increased (Supplementary Fig.1A). The results of MbSUS, BiFC, LCI, and pull-down assays revealed that the NRT1.2 loop region interacted with the CEPR2 kinase domain *in vitro* and in plant cells (Fig. 1). Four ABA importers (AITs) have previously been identified (Huang et al., 1999; Kanno et al., 2012). However, the MbSUS assay showed that CEPR2 interacted only with NRT1.2/NPF4.6 (AIT1), not with the other three AITs or with ABCG transporters (Fig. 1F). Blastp analysis revealed that the phosphorylation site in the loop region of NRT1.2/NPF4.6 is also present in AIT2 and AIT3, but not in AIT4 (Fig. S1B). Therefore, the details of the interaction between NRT1.2/NPF4.6 and CEPR2 remain to be fully elucidated.

The genetic analysis indicated that NRT1.2/NPF4.6 is epistatically and negatively regulated by CEPR2 (Fig. 2D-F). In most cases, protein phosphorylation rapidly and efficiently modifies target proteins in response to environmental stimuli (Grondin et al., 2015). Under normal conditions, CEPR2 promoted NRT1.2/NPF4.6 degradation, which was inhibited by ABA (Fig. 3). Furthermore, CEPR2 phosphorylated NRT1.2/NPF4.6 at S292 but not at S277, and non-phosphorylatable NRT1.2^{S292A} significantly inhibited NRT1.2/NPF4.6 degradation (Fig. 3). Together results indicated that CEPR2 phosphorylates NRT1.2/NPF4.6 at S292, thereby decreasing its stability. ABA strongly inhibited NRT1.2/NPF4.6 degradation (Fig. 3 and Fig. 5B). CEPR2 has similar effects on ABA receptors such as PYL4, and ABA inhibits the CEPR2-mediated phosphorylation of PYL4 (Yu et al., 2019). Therefore, ABA may also inhibit the CEPR2-mediated phosphorylation of NRT1.2/NPF4.6. Transporter activity can be regulated via the phosphorylation of proteins such as SOS1 (Quintero et al., 2011) and PIP2;1 (Grondin et al., 2015). Transport activity assays in yeast and *Xenopus* oocytes indicated that CEPR2-mediated phosphorylation of NRT1.2/NPF4.6 eliminated its ABA import activity. However, in the presence of ABA, non-phosphorylated NRT1.2/NPF4.6 was stable and retained the ability to import ABA into cells (Fig. 4). The elevated concentrations of intracellular ABA were recognized by the non-phosphorylated PYLs, eventually stimulating ABA signaling. Thus, CEPR2-mediated phosphorylation of PYLs and NRT1.2 balances the ABA response and plant growth (Fig. 7).

Further investigation revealed that degradation of NRT1.2/NPF4.6 was significantly inhibited by MG132 and E64d, alone or in combination (Fig. 5A, B), suggesting that NRT1.2/NPF4.6 degradation is mediated by both the 26S proteasome and vacuolar pathways. Y2H and pull-down assays showed that UBC32, UBC33, and UBC34 interacted with NRT1.2/NPF4.6 (Fig. 5C, D), and *in vitro* or semi-*in vivo* ubiquitination assays indicated that UBC32, UBC33, and UBC34 ubiquitinated themselves as well as NRT1.2/NPF4.6 (Fig. 5E, F). Genetic analyses showed that NRT1.2/NPF4.6 was epistatically and negatively regulated by UBC32, UBC33, and UBC34 in response to ABA (Fig. 6). Together, these results demonstrate that the three UBCs mediate the ubiquitination and degradation of NRT1.2/NPF4.6. UBC32 is a functional E2 that negatively regulates salt tolerance in *Arabidopsis* (Cui et al., 2012b). AtUBC32 is localized in the membrane of the endoplasmic reticulum (ER), where it participates in ER-associated degradation (ERAD) (Cui et al., 2012a). The ERAD process consists of substrate recognition, targeting, retrotranslocation, polyubiquitination, and degradation by the 26S proteasome (Cui et al., 2012a). UBC32, UBC33, and UBC34 are closely related proteins (Cui et al., 2012b). UBC34 from *Populus tomentosa* (PtoUBC34) also localizes in the ER membrane, where it interacts with the transcriptional repressors PtoMYB221 and PtoMYB156 (Zheng et al., 2019). This specific interaction allows translocation of PtoMYB221 and PtoMYB156 to the ER, thereby decreasing their suppression of genes involved in lignin biosynthesis (Zheng et al., 2019). The translocation of PtoMYB221 and PtoMYB156 to the ER by ER-localized UBC34 suggests that the two proteins might be degraded via the ERAD pathway. Furthermore, AtUBC34 triggers the turnover of SUCROSE TRANSPORTER 2 (SUC2) in response to light and ubiquitinated SUC2 *in vitro* (Xu et al., 2020). Recently, VPS23a, an E2-like protein, was identified as a key component of the endosomal sorting complex required for transport (ESCRTs) machinery I and shown to promote the vacuolar degradation of PYL4 (Dong et al., 2020; Yu et al., 2016). The localization of NRT1.2-GFP was observed on both PM and ER membrane despite of the presence of ABA or MG132 and E64d, despite of the presence of ABA or MG132 and E64d, that of NRT1.2^{S292A}-GFP was observed on the PM, whereas NRT1.2^{S292A}-GFP and NRT1.2^{S292D}-GFP was observed on PM or ER membrane only under overexposure conditions (Supplementary Figure 6), indicating that the phosphorylation of NRT1.2 changed its localization from PM to ER membrane to degradation. BiFC assays, in conjunction with ER-tracker in the presence of MG132 and E64d, showed that NRT1.2/NPF4.6 and UBC32, UBC33, and UBC34 interacted on the ER membrane (Fig. 5E). These data suggested that NRT1.2/NPF4.6 was ubiquitinated by UBC32, UBC33, and UBC34 on the ER membrane, and then degraded via the 26S proteasome and vacuolar degradation pathways.

Nonetheless, almost half of NRT1.2/NPF4.6 was degraded in the *cepr2-1* mutant (Fig. 3A, B), and CEPR2 did not phosphorylate Ser^{277} in NRT1.2/NPF4.6 (Fig. 3C, D). In addition, phosphorylation of NRT1.2/NPF4.6 at Ser^{277} might not affect its ABA import activity, as indicated by ABA transport assays in yeast cells (Fig. 4A). Finally, based on the protein levels, NRT1.2/NPF4.6 degradation also occurred in the WT and *ubc323334* plants under normal conditions (Fig. 6E, F).

These data suggested that other components might mediate the phosphorylation and degradation of NRT1.2/NPF4.6 under normal conditions, and that NRT1.2/NPF4.6 might have functions beyond ABA import. To fully characterize the regulation of NRT1.2/NPF4.6 phosphorylation, degradation, and function, other proteins that interact with NRT1.2/NPF4.6 must be identified and characterized.

In summary, our results show that the phosphorylation and ubiquitination of NRT1.2/NPF4.6, mediated by CEPR2 and UBCs, regulate ABA influx and plant growth in *Arabidopsis* (Fig. 7). Under normal conditions, CEPR2 phosphorylates NRT1.2/NPF4.6 and PYLs at the plasma membrane. The phosphorylated proteins are then translocated to the ER, where they are ubiquitinated by UBC32, UBC33, and UBC34. Finally, ubiquitinated NRT1.2/NPF4.6 and PYLs are degraded by the 26S proteasome and vacuolar degradation pathways, allowing seed germination and primary root growth. However, when excess ABA is present, the phosphorylation of NRT1.2/NPF4.6 and PYLs by CEPR2 is inhibited, resulting in stabilization of NRT1.2/NPF4.6 and PYL and maintenance of their activities. Thus, NRT1.2/NPF4.6 imports ABA into the cell, where PYLs bind ABA to transduce the ABA signal. The resultant ABA response inhibits seed germination and primary root growth.

Materials and Methods

Plant materials and growth conditions

Arabidopsis thaliana (L.) Heynh. cv. 'Columbia-0' was used as the WT line. The T-DNA insertion lines, SALK_072696 (*nrt1.2-1*) and SALK_011182 (*nrt1.2-2*), both in the Col-0 background, were obtained from the *Arabidopsis* Biological Resource Center (http://www.arabidopsis.org). The *cepr2-1* T-DNA insertion mutant and the CEPR2-overexpressing line *CEPR2-OE-9* were characterized previously (Yu et al., 2019). The homozygous single and double mutants (*cepr2-1*, *nrt1.2-1*, and *cepr2-1nrt1.2-1*) were verified using RT-PCR with the primers listed in Supplementary Table 2. The complemented *nrt1.2-1* seedlings with point mutations at Ser^{292} to alanine or to aspartate were designated *NRT1.2*^{S292A}*-COM* and *NRT1.2*^{S292D}*-COM*, respectively. *NRT1.2/NPF4.6-OE*, *NRT1.2-COM*, *NRT1.2*^{S292A}*-COM*, and *NRT1.2*^{S292D}*-COM* seedlings were selected on 1/2 Murashige and Skoog (MS) medium (1.5% sucrose and 0.85% agar) supplemented with 50 mg/L kanamycin. *NRT1.2/NPF4.6* expression levels in transgenic seedlings were confirmed with RT-PCR using the primers listed in Supplementary Table 2. All selected *Arabidopsis* plants were grown in a greenhouse under a 16 h light/8 h dark cycle at 23°C with a light intensity of 9600 LUX.

Phosphoproteome analysis

Protein extraction and phosphoproteome analysis were performed as previously described (Pi et al., 2016). Total proteins were extracted from *CEPR2-OE-9* and WT seedlings grown in 1/2 MS for 7 d using the TCA/acetone method (Wisniewski et al., 2009). Phosphoproteome analysis was performed using CapitalBio technology (Beijing, China). Mass spectrometry data were deposited in the ProteomeXchange Consortium via the PRIDE partner repository (dataset identifier PXD021458; http://www.ebi.ac.uk/pride).

MbSUS, BiFC, and LCI assays

The MbSUS assay was performed as described previously (Obrdlik et al., 2004); detailed descriptions of associated experimental principles and methods are given in Yu et al. (Yu et al., 2019). In brief, for Nub fusions, PCR products were cloned and transformed with pNXgate, cleaved with *Eco*RI and *Sma*I, and transformed into the yeast strain THY.AP5. Strains were selected on synthetic dropout (SD) medium lacking tryptophan (W) and uracil (U). For Cub fusions, PCR products were cloned and transformed with pMetYCgate, cleaved with *Pst*I/*Hind*III, and transformed (along with PCR products) into the yeast strain THY.AP4. Transformants were further selected on SD medium lacking leucine (L). Clones from each transformant were incubated on SD media lacking leucine, tryptophan, and uracil (SD-Trp/-Leu/-Ura; SD-WLU) at 30°C for 3 days. To detect protein interactions, colonies were spotted onto control media (SD-WLU), as well as onto

selection media lacking leucine, tryptophan, uracil, adenine, and histidine (SD-Trp/-Leu/-Ura/-Ade/-His; SD-WLUAH). Colony growth was monitored for 3-6 days.

Luciferase complementary imaging (LCI) assays were performed as previously described (Chen et al., 2008; Xu et al., 2018). In brief, the full-length CDS of *CEPR2* was cloned into vector pCAMBIA1300-nLUC (nLUC) to generate the CEPR2-nLUC construct, and the full-length CDS of *NRT1.2/NPF4.6* was cloned into vector pCAMBIA1300-cLUC (cLUC) to generate the NRT1.2-cLUC construct. Next, 1 mL of *Agrobacterium tumefaciens* cells harboring CEPR2-nLUC, NRT1.2-cLUC, or nLUC were mixed to obtain the following combinations, each with a final optical density at 600 nm (OD_{600}) of 1.0: CEPR2-nLUC+cLUC, NRT1.2-cLUC+nLUC, and CEPR2-nLUC+NRT1.2-cLUC. Each of these combinations of *A. tumefaciens* cells were separately infiltrated into *N. benthamiana* leaves. *N. benthamiana* plants were grown at 26°C for 60 h. Five minutes before detection, 0.2 mM luciferin (Promega, Madison, WI, USA) was sprayed on the treated leaves, and luciferase activity was measured using a cooled charge-coupled device (Lumina II system, Perkin Elmer, Waltham, MA, USA).

BiFC assays were performed as described previously (Waadt and Kudla, 2008). In brief, the full-length CDS of *CEPR2* (without the stop codon) was cloned into vector pSPYNE-35S to generate the CEPR2-YFP^N construct, and the full-length CDS of *NRT1.2/NPF4.6* (without the stop codon) was cloned into vector pSPYCE-35S to obtain the NRT1.2-YFP^C construct. *A .tumefaciens* cells harboring CEPR2-YFP^N and NRT1.2-YFP^C were mixed with 10 mL of MMA medium (10 mM $MgCl_2$, 50 mM MES, and 20 μM acetosyringone, pH 5.6) to yield a final OD_{600} of 1.0. The cell mixtures were injected into *N. benthamiana* leaves by gently pressing a disposable syringe to the abaxial surface of a fully-expanded leaf (approximate width: 3 cm at the midpoint). Plants were grown at 26°C for 36-60 h, and then YFP signals in the leaves were detected at 488 nm using an LSM51 Confocal Laser Scanning Microscope (Zeiss, Germany). The amphiphilic styryl dye FM4-64 [N-(3-triethylammomiumpropyl) 4-(p-diethylaminophenylhexatrienyl)] was used as a plasma membrane marker.

Pull-down assay

To characterize interactions among CEPR2, UBCs, and NRT1.2/NPF4.6, the CDS encoding the cytosol loop region (232-346 aa) of NRT1.2/NPF4.6^{loop} was fused with GST in vector pGEX-4T-1 to generate pGEX-4T-1-GST-NRT1.2^{loop} (NRT1.2^{loop} -GST); the full-length CDSs of the UBCs (without the transmembrane domains) were fused with the His tag in vector pET30a-His to generate pET30a-His-UBC32$^{\Delta TM}$-His, pET30a-His-UBC33$^{\Delta TM}$-His, and pET30a-His-UBC34$^{\Delta TM}$-His; and the kinase domain (642-977 aa) of CEPR2 was fused with His tag in the pET30a-His vector to generate pET30a-His-CEPR2^{KD}-His (CEPR2^{KD}-His). The resultant NRT1.2^{loop}-GST and CEPR2^{KD}-His constructs were transformed into competent *E. coli* Rosetta cells. The transformed cells were cultured in 500 mL Luria-Bertani medium at 37°C to an OD_{600} of 1.0. Protein expression was then induced with 0.8 mM isopropyl β-D-thiogalactoside (IPTG) for 12 h at 16°C.

Next, *E. coli* cells were obtained by centrifugation at 6000 rpm for 5 min at 4°C. The pellet was resuspended in 5 mL ddH_2O. Lysates were obtained by ultrasonication (JY92-II, Scientz Biotechnology Co., Ltd, Ningbo, China) with the following parameters: operating power, 300 w; working time, 10 s; interval time, 5 s; and cycles, 30. Lysates were clarified by centrifugation at 8000 rpm for 10 min at 4°C. The CEPR2^{KD}-His protein was purified using the His-Tagged Protein Purification Kit (CWBIO, Beijing, China), and NRT1.2^{loop}-GST was purified using Pierce Glutathione Spin Columns (Thermo Fisher Scientific, Waltham, MA, USA). In the pull-down assay, 50 µg NRT1.2^{loop}-GST and 50 µg CEPR2^{KD}-His were incubated in 1 mL of binding buffer (50 mM Tris-HCl, 150 mM NaCl, pH 8.0) at 4°C for 2 h with constant slight shaking. After incubation, GST proteins were purified with Pierce Glutathione Spin Columns, eluted, and analyzed using anti-His antibodies (CWBIO, Beijing, China). The primers used in this experiment are listed in Supplementary Table 2.

RNA extraction, RT-PCR, and quantitative RT-PCR (qRT-PCR)

Total RNAs from 7-day-old seedlings grown on 1/2 MS with or without 1 µM ABA were extracted using TRIzol (Invitrogen, Carlsbad, CA, USA) or Universal Plant Total RNA Extraction Kits (Spin-column)-I (BioTeke, Beijing, China). The cDNA used for qRT-PCR was synthesized using PrimeScript reverse transcriptase with oligo dT primer and Prime Script RT Enzyme MIX I (Accurate Biotechnology (human) Co.,Ltd). qRT -PCRs were performed using the ChamQ Universal SYBR qPCR Master Mix (Vazyme, Biotech Co., Ltd) on a CFX96 instrument (Bio-Rad, Hercules, CA, USA). *UBC21* and *UBQ10* were used as internal controls for qRT-PCR. The cDNA used for RT-PCR was synthesized using PrimeScript First-Strand cDNA Synthesis Kit (Takara, Osaka, Japan). RT-PCR cycling conditions were as follows: denaturation at 94°C for 5 min, followed by 23-34 cycles of amplification, and final elongation at 72°C for 5 min. *EF-1α* was used as the internal control for RT-PCR. The primers used are listed in Supplementary Table 2.

Germination and root length measurements

Plants with different genotypes were grown under the same conditions in the greenhouse, and all seeds were harvested simultaneously. Germination assays were performed as previously described (Chen et al., 2014). In brief, the seeds were surface-sterilized and incubated in the dark at 4°C for 3 days on 1/2 MS medium with or without 1 µM ABA. Germination, defined as the emergence of the radicle through the seed coat, was assessed every 12 h. At the end of the third day, germination rates were calculated. To assess growth, sterilized seeds were grown vertically for 7 days on 1/2 MS medium with or without 1 µM ABA. The root lengths of at least 20 seedlings per line (WT, mutant, and transgenic) were measured using a ruler, and mean root length was calculated for each line.

Cell-free degradation

To investigate the effects of CEPR2 on NRT1.2/NPF4.6, NRT1.2^{loop}-GST protein levels were determined after incubation with total protein extracts from *CEPR2-OE-9*, *cepr2-1*, or WT seedlings grown on 1/2 MS medium with or without 1 μM ABA. Total proteins were extracted from 0.4 g samples of 7-day-old seedlings of all genotypes using 600 μL extraction buffer (5 mM DTT, 10 mM NaCl, 25 mM Tris-HCl [pH 7.5], 10 mM ATP, 4 mM PMSF, and 10 mM $MgCl_2$). The crude extracts were held on ice (4°C) for 30 min and centrifuged twice at 12,000 rpm for 10 min at 4°C. After centrifugation, the supernatants were collected. About 0.5 mg of purified NRT1.2-GST was incubated with total protein extracts for 0, 10, 30, or 60 min at 22°C. At each time point, 20 μL of each solution was transferred to a new centrifuge tube, combined with 5 μL of 5× loading buffer, and boiled for 5 min to terminate the reaction. The level of the NRT1.2/NPF4.6 protein in each reaction was determined using anti-GST antibodies. Spot densitometry was performed using ImageJ v1.36 (http://rsb.info.nih.gov/ij/). To investigate the NRT1.2/NPF4.6 degradation pathway, protein extracts with 100 μM MG132 (an inhibitor of the 26S proteasome pathway) and/or 100 μM E64d (an inhibitor of the vacuolar degradation pathway) were incubated with purified NRT1.2^{loop}-GST fusion proteins. Protein levels were detected using anti-GST antibodies (TransGen Biotech). ImageJ v1.36 was used to quantify the intensity of each protein band.

In vitro kinase assay

To investigate possible sites at which CEPR2 phosphorylated NRT1.2/NPF4.6, *in vitro* kinase assays were carried out. The CDSs encoding the mutant loop region (aa 232-346) of NRT1.2/NPF4.6, in which Ser^{277} or Ser^{292} were point mutated to alanine (A) or aspartate (D), were fused with the GST tag in the pGEX-4T-1 vector to generate pGEX-4T-1-GST-NRT1.2$^{loopS277A/D}$ (NRT1.2$^{loopS277A/D}$-GST) and pGEX-4T-1-GST-NRT1.2$^{loopS292A/D}$ (NRT1.2$^{loopS292A/D}$-GST). Transformation, induction, and purification of these fusion proteins were performed as described above. CEPR2-GFP was purified using affinity chromatography. *In vitro* kinase assays were carried out using purified CEPR2-GFP and NRT1.2^{loop}-GST, NRT1.2^{loopS277A}-GST, or NRT1.2^{loopS292A}-GST. Fifty micrograms of NRT1.2^{loop}-GST, NRT1.2^{loopS277A}-GST, or NRT1.2^{loopS292A}-GST was combined with 0.5 μg CEPR2-GFP in 50 μL of reaction buffer (25 mM HEPES, pH 7.2, 1 mM DTT, 50 mM NaCl, 2 mM EGTA, 5 mM $MgSO_4$, and 50 μM ATP). The reaction mixtures were incubated at 30°C for 0-120 min, and the reaction was terminated by addition of 5× loading buffer. Unincubated reaction mixture (at 0 min) was used as the negative control. Proteins were then fractionated by sodium dodecyl sulfate polyacrylamide gel electrophoresis (SDS-PAGE) and Mn^{2+}-Phos-tag-PAGE (50 μM Phos-tag and 100 μM Mn^{2+}). After 30 min incubation at 37°C, 0.01 U/μL CIAP (Promega, Madison, WI, USA) was added to the reaction buffer, and the mixture was incubated for another 30 min at 37°C to remove the phosphoryl group(s) of NRT1.2^{loop}. To determine the effects of ABA on the phosphorylation of NRT1.2/NPF4.6, *in vitro* kinase assays were performed using purified CEPR2^{KD}-His and

NRT1.2^{loop}-GST with or without 10 μM ABA in the presence of 100 μM MG132 or 100 μM E64d. Primers used in this experiment are listed in Supplementary Table 2.

Analysis of ABA import activity in a yeast system

The CDSs of PYR1 and ABI1 were amplified by PCR and inserted into plasmids pGBKT7 and pGADT7, respectively. The resultant plasmids were co-transformed into *Saccharomyces cerevisiae* Yeast Gold cells. Successfully transformed colonies were identified on SD media lacking Leu and Trp (SD-WL). To detect ABA import activity levels, pYES2 plasmids or plasmids containing the full-length CDS of NRT1.2/NPF4.6, NRT1.2^{S292A}, or NRT1.2^{S292D} were separately transformed into yeast cells. Successfully transformed colonies were identified on SD-WLU media, and then transferred to SD-WLUAH media in the absence or presence of 1 μM ABA. Because the growth of the transformed yeast cells depended on ABA levels, ABA import activity could be quantified by observing the growth of the transformed cells. Growth was photographed after 2-3 days of culture. Yeast transformants were transferred to 5 mL of SD-WLUAH liquid medium and incubated at 30°C for 8 h in a shaker. Absorbance at 600 nm was measured using a spectrophotometer (T6, Pgeneral, Beijing, China). Twelve replicates were performed for each co-transformation, and mean values were calculated. Primers used in this experiment are listed in Supplementary Table 2.

Quantification of NRT1.2/NPF4.6 transporter activity in *Xenopus* oocytes

To further test the effects of CEPR2 phosphorylation on NRT1.2/NPF4.6-mediated ABA import, we measured the levels of ABA transport activity associated with NRT1.2/NPF4.6, non-phosphomimic NRT1.2/NPF4.6 (NRT1.2^{S292A}), and phosphomimic NRT1.2/NPF4.6 (NRT1.2^{S292D}) in *Xenopus* oocytes. The QuikChange Lightning site-directed mutagenesis kit (Agilent Technologies, CA, USA) was used to generate NRT1.2^{S292A} and NRT1.2^{S292D}, which were then cloned into the expression vector pT7TS. The pT7TS-derived plasmids were linearized by *Bam*HI, and the RNA was transcribed *in-vitro* using the mMESSAGE mMACHINET7 mRNA synthesis kit (Ambion). Primers used in these experiments are listed in Supplementary Table 2. *Xenopus* oocytes were isolated in 25 mL of ND96 solution containing 43 mg collagenase and 12.5 mg trypsin inhibitor for 1.5 h. After isolation, cells were recovered in 25 mL of ND96 for another 24 h. The *Xenopus* oocytes were then injected with 20 ng of NRT1.2/NPF4.6, NRT1.2^{S292A}, NRT1.2^{S292D}, AIT3, and/or CEPR2^{KD} cRNA. The injected oocytes were incubated with the Modified Barth's solution (MBS) (88 mM NaCl, 1 mM KCl, 0.71 mM $CaCl_2$, 0.82 mM $MgSO_4 \cdot 7H_2O$, 2.4 mM $NaHCO_3$, 15 mM HEPES) at pH 7.4 with or without 10 μM ABA for 6 h, and then the *Xenopus* oocytes were washed five times with MBS. ABA contents in the *Xenopus* oocytes were measured using liquid chromatography-tandem mass spectrometry (LC-MS/MS)

Analysis of NRT1.2/NPF4.6 transporter activity *in planta*

To investigate the effects of NRT1.2/NPF4.6 phosphorylation on ABA import *in planta*, transgenic *nrt1.2-1* mutant carrying native promoter-driven normal NRT1.2/NPF4.6 (*NRT1.2-COMs*), NRT1.2/NPF4.6 not phosphorylated at Ser^{292} (*NRT1.2*^{S292A}*-COMs*), and NRT1.2/NPF4.6 phosphorylated at Ser^{292} (*NRT1.2*^{S292D}*-COM*) were generated as described above. To measure ABA content, various seedlings (i.e., the *NRT1.2*^{S292A}*-COM-8*, *NRT1.2*^{S292D}*-COM-2*, and *nrt1.2-1* mutants, *NRT1.2-OE-1*, and WT) were grown on 1/2 MS with or without 1 μM ABA for 7 days. The ABA contents in the seedlings were measured as previously described (Xu et al., 2016).

Ubiquitination assays

The constructs pET30a-His-UBC32$^{\Delta TM}$-His, pET30a-His-UBC33$^{\Delta TM}$-His, and pET30a-His-UBC34$^{\Delta TM}$-His, as well as the corresponding mutant fusion proteins, were expressed and purified as described above. The thioester assay reaction was performed in a 60 μL reaction volume containing 50 mM Tris-HCl (pH 7.4), 10 mM $MgCl_2$, 10 mM ATP, 100 ng UBE1 (Boston Biochemicals, Cambridge, MA, USA), 10 μg recombinant, and 10 μg pET30a-His-UBC33$^{\Delta TM}$-His, pET30a-His-UBC32$^{\Delta TM}$-His pET30a-His-UBC34$^{\Delta TM}$-His, or the corresponding mutant recombinant Ub-Myc (Boston Biochemicals, Cambridge, MA, USA). Reactions were split after incubation for 6-24 h at 30°C and terminated by addition of SDS sample buffer without dithiothreitol (DTT). Samples were separated on 10% SDS-PAGE gels after boiling at 100°C for 5 min, and then visualized using western blots with anti-His and anti-Myc.

Total membrane proteins isolated from the *NRT1.2-OE-1/ubc323334* mutant were incubated with purified UBCs. Immunoprecipitation and immunoblot analyses were performed as described above. Monoclonal anti-NRT1.2/NPF4.6 antibody (Sangon Biotech China) was used to detect ubiquitinated proteins.

Author contributions

C.W., C.Z., and Z.Y. conceived the original screening and research plans; L.Z., Z.Y., X.Y., Y.M., and Y.R. performed experiments, analyzed the data, made the figures, and wrote the original article; G.Y., S.Z., J.H., and K.Y. provided suggestions; C.W. and C.Z. supervised and complemented the writing. All authors read and approved the final manuscript.

Acknowledgments

This work was supported by the Major Program of Shandong Province Natural Science Foundation (ZR2018ZB0212), Shandong Province Natural Science Foundation (ZR2020QC036), the National Key R&D Program of China (2018YFD1000704, 2018YFD1000700), and the Natural Science Foundation of China (Grant number 31970292, 31570271, 32000225). We thank Prof. Yi Wang (Chinese Agricultural University) for the measurement of NRT1.2/NPF4.6 transporter activity in *Xenopus* oocyte cells, and Prof. Kim Woo Taek for donating the *ubc323334* triple mutant from Yonsei University. We also thank Jie Dai at Shanghai Bioprofile Technology Company Ltd. for his technical support in

mass spectroscopy and LetPub (https://www.letpub.com/) for its linguistic assistance during the preparation of this manuscript.

Conflict of interest

The authors declare that they have no conflict of interest.

Data availability

All relevant data, vectors, and plant materials that support the findings of this study are available from the corresponding author upon request.

497 **References**

498 Boursiac, Y., Leran, S., Corratge-Faillie, C., Gojon, A., Krouk, G., and Lacombe, B. (2013). ABA transport
499 and transporters. Trends Plant Sci 18:325-333.
500 Chen, C., Wu, C., Miao, J., Lei, Y., Zhao, D., Sun, D., Yang, G., Huang, J., and Zheng, C. (2014).
501 Arabidopsis SAG protein containing the MDN1 domain participates in seed germination and
502 seedling development by negatively regulating ABI3 and ABI5. Journal of experimental botany
503 65:35-45.
504 Chen, H., Zou, Y., Shang, Y., Lin, H., Wang, Y., Cai, R., Tang, X., and Zhou, J.M. (2008). Firefly
505 luciferase complementation imaging assay for protein-protein interactions in plants. Plant
506 Physiol 146:368-376.
507 Chen, H.H., Qu, L., Xu, Z.H., Zhu, J.K., and Xue, H.W. (2018). EL1-like Casein Kinases Suppress ABA
508 Signaling and Responses by Phosphorylating and Destabilizing the ABA Receptors PYR/PYLs in
509 Arabidopsis. Mol Plant 11:706-719.
510 Cui, F., Liu, L., Li, Q., Yang, C., and Xie, Q. (2012a). UBC32 mediated oxidative tolerance in Arabidopsis.
511 J Genet Genomics 39:415-417.
512 Cui, F., Liu, L., Zhao, Q., Zhang, Z., Li, Q., Lin, B., Wu, Y., Tang, S., and Xie, Q. (2012b). Arabidopsis
513 ubiquitin conjugase UBC32 is an ERAD component that functions in brassinosteroid-mediated
514 salt stress tolerance. Plant Cell 24:233-244.
515 Cutler, S.R., Rodriguez, P.L., Finkelstein, R.R., and Abrams, S.R. (2010). Abscisic acid: emergence of a
516 core signaling network. Annu Rev Plant Biol 61:651-679.
517 Dong, W., Zhu, Y., Chang, H., Wang, C., Yang, J., Shi, J., Gao, J., Yang, W., Lan, L., Wang, Y., et al.
518 (2020). An SHR–SCR module specifies legume cortical cell fate to enable nodulation. Nature.
519 Grondin, A., Rodrigues, O., Verdoucq, L., Merlot, S., Leonhardt, N., and Maurel, C. (2015). Aquaporins
520 Contribute to ABA-Triggered Stomatal Closure through OST1-Mediated Phosphorylation. Plant
521 Cell 27:1945-1954.
522 Huang, N.C., Liu, K.H., Lo, H.J., and Tsay, Y.F. (1999). Cloning and functional characterization of an
523 Arabidopsis nitrate transporter gene that encodes a constitutive component of low-affinity
524 uptake. Plant Cell 11:1381-1392.
525 Kang, J., Yim, S., Choi, H., Kim, A., Lee, K.P., Lopez-Molina, L., Martinoia, E., and Lee, Y. (2015).
526 Abscisic acid transporters cooperate to control seed germination. Nat Commun 6:8113.
527 Kanno, Y., Hanada, A., Chiba, Y., Ichikawa, T., Nakazawa, M., Matsui, M., Koshiba, T., Kamiya, Y., and
528 Seo, M. (2012). Identification of an abscisic acid transporter by functional screening using the
529 receptor complex as a sensor. Proc Natl Acad Sci U S A 109:9653-9658.
530 Kuromori, T., Miyaji, T., Yabuuchi, H., Shimizu, H., Sugimoto, E., Kamiya, A., Moriyama, Y., and
531 Shinozaki, K. (2010). ABC transporter AtABCG25 is involved in abscisic acid transport and
532 responses. Proc Natl Acad Sci U S A 107:2361-2366.
533 Kuromori, T., Seo, M., and Shinozaki, K. (2018). ABA Transport and Plant Water Stress Responses.
534 Trends Plant Sci 23:513-522.
535 Leran, S., Noguero, M., Corratge-Faillie, C., Boursiac, Y., Brachet, C., and Lacombe, B. (2020).
536 Functional Characterization of the Arabidopsis Abscisic Acid Transporters NPF4.5 and NPF4.6 in
537 Xenopus Oocytes. Frontiers in plant science 11.
538 Li, W., Song, T., Wallrad, L., Kudla, J., Wang, X., and Zhang, W. (2019). Tissue-specific accumulation of
539 pH-sensing phosphatidic acid determines plant stress tolerance. Nat Plants 5:1012-1021.
540 Obrdlik, P., El-Bakkoury, M., Hamacher, T., Cappellaro, C., Vilarino, C., Fleischer, C., Ellerbrok, H.,
541 Kamuzinzi, R., Ledent, V., Blaudez, D., et al. (2004). K+ channel interactions detected by a
542 genetic system optimized for systematic studies of membrane protein interactions. Proc Natl
543 Acad Sci U S A 101:12242-12247.
544 Pi, E., Qu, L., Hu, J., Huang, Y., Qiu, L., Lu, H., Jiang, B., Liu, C., Peng, T., Zhao, Y., et al. (2016).
545 Mechanisms of Soybean Roots' Tolerances to Salinity Revealed by Proteomic and
546 Phosphoproteomic Comparisons Between Two Cultivars. Mol Cell Proteomics 15:266-288.
547 Quintero, F.J., Martinez-Atienza, J., Villalta, I., Jiang, X., Kim, W.Y., Ali, Z., Fujii, H., Mendoza, I., Yun,
548 D.J., Zhu, J.K., et al. (2011). Activation of the plasma membrane Na/H antiporter

549 Salt-Overly-Sensitive 1 (SOS1) by phosphorylation of an auto-inhibitory C-terminal domain. Proc
550 Natl Acad Sci U S A 108:2611-2616.
551 Raghavendra, A.S., Gonugunta, V.K., Christmann, A., and Grill, E. (2010). ABA perception and
552 signalling. Trends Plant Sci 15:395-401.
553 Soma, F., Mogami, J., Yoshida, T., Abekura, M., Takahashi, F., Kidokoro, S., Mizoi, J., Shinozaki, K., and
554 Yamaguchi-Shinozaki, K. (2017). ABA-unresponsive SnRK2 protein kinases regulate mRNA
555 decay under osmotic stress in plants. Nat Plants 3:16204.
556 Teardo, E., Carraretto, L., Moscatiello, R., Cortese, E., Vicario, M., Festa, M., Maso, L., De Bortoli, S.,
557 Cali, T., Vothknecht, U.C., et al. (2019). A chloroplast-localized mitochondrial calcium uniporter
558 transduces osmotic stress in Arabidopsis. Nat Plants 5:581-588.
559 Waadt, R., and Kudla, J. (2008). In Planta Visualization of Protein Interactions Using Bimolecular
560 Fluorescence Complementation (BiFC). CSH Protoc 2008:pdb prot4995.
561 Wang, P., Zhao, Y., Li, Z., Hsu, C.C., Liu, X., Fu, L., Hou, Y.J., Du, Y., Xie, S., Zhang, C., et al. (2018).
562 Reciprocal Regulation of the TOR Kinase and ABA Receptor Balances Plant Growth and Stress
563 Response. Mol Cell 69:100-112 e106.
564 Wisniewski, J.R., Zougman, A., Nagaraj, N., and Mann, M. (2009). Universal sample preparation
565 method for proteome analysis. Nature methods 6:359-362.
566 Xu, Q., Truong, T.T., Barrero, J.M., Jacobsen, J.V., Hocart, C.H., and Gubler, F. (2016). A role for
567 jasmonates in the release of dormancy by cold stratification in wheat. J Exp Bot 67:3497-3508.
568 Xu, Q., Yin, S., Ma, Y., Song, M., Song, Y., Mu, S., Li, Y., Liu, X., Ren, Y., Gao, C., et al. (2020). Carbon
569 export from leaves is controlled via ubiquitination and phosphorylation of sucrose transporter
570 SUC2. Proc Natl Acad Sci U S A 117:6223-6230.
571 Xu, Y., Yu, Z., Zhang, D., Huang, J., Wu, C., Yang, G., Yan, K., Zhang, S., and Zheng, C. (2018). CYSTM,
572 a Novel Non-Secreted Cysteine-Rich Peptide Family, Involved in Environmental Stresses in
573 Arabidopsis thaliana. Plant & cell physiology 59:423-438.
574 Yang, G., Yu, Z., Gao, L., and Zheng, C. (2019). SnRK2s at the Crossroads of Growth and Stress
575 Responses. Trends Plant Sci 24:672-676.
576 Yu, F., Lou, L., Tian, M., Li, Q., Ding, Y., Cao, X., Wu, Y., Belda-Palazon, B., Rodriguez, P.L., Yang, S., et
577 al. (2016). ESCRT-I Component VPS23A Affects ABA Signaling by Recognizing ABA Receptors
578 for Endosomal Degradation. Mol Plant 9:1570-1582.
579 Yu, Z., Duan, X., Luo, L., Dai, S., Ding, Z., and Xia, G. (2020). How Plant Hormones Mediate Salt Stress
580 Responses. Trends Plant Sci 25:1117-1130.
581 Yu, Z., Zhang, D., Xu, Y., Jin, S., Zhang, L., Zhang, S., Yang, G., Huang, J., Yan, K., Wu, C., et al. (2019).
582 CEPR2 phosphorylates and accelerates the degradation of PYR/PYLs in Arabidopsis. J Exp Bot.
583 Zakrzewska, S., Mehdipour, A.R., Malviya, V.N., Nonaka, T., Koepke, J., Muenke, C., Hausner, W.,
584 Hummer, G., Safarian, S., and Michel, H. (2019). Inward-facing conformation of a multidrug
585 resistance MATE family transporter. Proceedings of the National Academy of Sciences of the
586 United States of America 116:12275-12284.
587 Zhang, H., Li, Y., and Zhu, J.K. (2018). Developing naturally stress-resistant crops for a sustainable
588 agriculture. Nat Plants 4:989-996.
589 Zhang, H., Zhu, H., Pan, Y., Yu, Y., Luan, S., and Li, L. (2014). A DTX/MATE-type transporter facilitates
590 abscisic acid efflux and modulates ABA sensitivity and drought tolerance in Arabidopsis. Mol
591 Plant 7:1522-1532.
592 Zheng, L., Chen, Y., Ding, D., Zhou, Y., Ding, L., Wei, J., and Wang, H. (2019). Endoplasmic
593 reticulum-localized UBC34 interaction with lignin repressors MYB221 and MYB156 regulates the
594 transactivity of the transcription factors in Populus tomentosa. BMC Plant Biol 19:97.

595

Supplementary data

Supplementary Figure 1. Interaction of 78 proteins with upregulated phosphorylation with CEPR2, as determined by MbSUS, and comparison of the C-terminal amino acids of NRT1.2 with those of other ABA transporters.

Supplementary Figure 2. The mRNA levels of various ABA transporters in *CEPR2-OE-9*, wild type (WT), and *cepr2-1* seedlings, with or without ABA, as determined by qRT-PCR.

Supplementary Figure 3. Codon-optimized sequence of the NRT1.2^{loop} domain.

Supplementary Figure 4. Phosphorylation of NRT1.2/NPF4.6 does not affect its interaction with CEPR2 and the ABA transport activity of NRT1.2^{S292D} or NRT1.2^{S292A} and AIT3.

Supplementary Figure 5. Construction of the genetic complementation of *nrt1.2-1*.

Supplementary Figure 6. Subcellular localization of NRT1.2-GFP, NRT1.2^{S292A}-GFP, and NRT1.2^{S292D}-GFP under 1/2 MS, 50 μM ABA or MG132+E64d in *Nicotiana benthamiana* leaves.

Supplementary Figure 7. Gene structure of the Group XIV ubiquitin-conjugating enzymes UBC32, UBC33, and UBC34.

Supplementary Table 1. Seventy-eight dramatically upregulated phosphoproteins identified using phosphorylation mass spectrometry.

Supplementary Table 2. Primers used in this study.

Supplementary Excel 1. Peptides differentially phosphorylated between *CEPR2-OE-9* and WT seedlings, identified by mass spectrometry.

Figure legends

Figure 1. CEPR2 interacts with the ABA importer NRT1.2/NPF4.6.

(A) Firefly luciferase complementation imaging assay showing the interactions between CEPR2 and NRT1.2/NPF4.6. A key to the combination shown in each quadrant is given above the image.

(B) Bimolecular fluorescence complementation (BiFC) assay showing the interaction between CEPR2 and NRT1.2/NPF4.6 in *Nicotiana benthamiana*. FM4-64, plasma membrane dye N-(3-triethylammomiumpropyl) 4-(p-diethylaminophenylhexatrienyl).

(C) Protein structures of CEPR2 and NRT1.2/NPF4.6. Phosphorylation sites S277 and S292, identified using phosphorylation mass spectrometry, are labeled on the NRT1.2/NPF4.6 protein. LRR, leucine-rich repeat receptor-like domain; KD, kinase domain; loop, loop domain of NRT1.2/NPF4.6; PM, plasma membrane.

(D) Mating-based split ubiquitin system (MbSUS) assay showing the functional domains of CEPR2 that interact with the loop region of N NRT1.2/NPF4.6 (NRT1.2^{loop}, aa 232-346).

(E) Pull-down assays using purified GST, NRT1.2^{loop}-GST, and CEPR2^{KD}-His expressed in *E. coli*.

(F) MbSUS assay showing the interactions between CEPR2 and eight characterized ABA importers, including NRT1.2/NPF4.6, ABA importer 2 (AIT2), AIT3, AIT4, ABC transporter G25 (ABCG25), ABCG30, ABCG31, and ABCG40.

Figure 2. CEPR2 negatively regulates NRT1.2/NPF4.6 to influence ABA signaling.

(A) NRT1.2/NPF4.6 transcript levels and protein levels in WT and transgenic *Arabidopsis* lines overexpressing NRT1.2/NPF4.6, as determined by RT-PCR and western blotting. *EF-1α* was used as the internal control for RT-PCR, and Rubisco large subunit (RbcL) was used as a loading control for western blots.

(B) Schematic illustration of the T-DNA insertion sites in the *nrt1.2-1* and *nrt1.2-2* mutants.

(C) NRT1.2/NPF4.6 transcript and protein levels in WT, *nrt1.2-1*, and *nrt1.2-2* seedlings.

(D) Phenotypes of the WT, *NRT1.2-OE*, *nrt1.2-1*, *nrt1.2-2*, *cepr2-1*, and *cepr2-1nrt1.2-1* seedlings grown for 7 days on 1/2 MS with or without 1 μM ABA.

(E) Lengths of primary roots of the seedlings shown in (D). Error bars indicate SEM (N = 3). Bars labeled with different lowercase letters are significantly different from one another ($P < 0.05$; one-way ANOVA).

(F) Germination rates of the seedlings shown in (D). Error bars indicate SEM (N = 3).

Figure 3. CEPR2 reduces NRT1.2/NPF4.6 stability depending on the phosphorylation of Serine 292 (Ser^{292}).

(A) Cell-free degradation of NRT1.2-GST in soluble protein extracts of *CEPR2-OE-9*, WT, and *cepr2-1* seedlings treated with or without 1 μM ABA. NRT1.2^{loop}-GST protein levels were quantified using anti-GST antibodies (indicated by red

arrows).

(B) Normalized plots of NRT1.2/NPF4.6 degradation, based on band intensities shown in (A). Error bars indicate SEM (N = 3).

(C) *In vitro* kinase assays showing the effects of CEPR2 on the phosphorylation of the loop regions of NRT1.2/NPF4.6 (NRT1.2^{loop}-GST, NRT1.2^{loop}S292A-GST, and NRT1.2^{loop}S277A-GST). NRT1.2/NPF4.6 phosphorylation status was detected based on the Phos-tag. Calf intestinal alkaline phosphatase (CIAP) was used to remove phosphate group(s) of the proteins.

(D) Normalized plot showing the relative contents of phosphorylated and non-phosphorylated NRT1.2/NPF4.6, based on the band intensities shown in (C). Error bars indicate SEM (N = 3). Bars labeled with different lowercase letters are significantly different from one another ($P < 0.05$; one-way ANOVA).

(E) Cell-free degradation assays showing the effects of ABA on the degradation of NRT1.2^{loop} and NRT1.2^{loopS292A} in soluble protein extracts from *CEPR2-OE-9* seedlings. NRT1.2^{loop}-GST and NRT1.2^{loopS292A}-GST were quantified by western blotting with anti-GST antibody. RbcL was used as the loading control.

(F) Normalized plot of NRT1.2/NPF4.6 contents based on the band intensities shown in (E). Error bars indicate SEM (N = 3).

Figure 4. Phosphorylation of NRT1.2/NPF4.6 at serine 292 dampens its ABA import activity.

(**A**) Y2H assays showing ABA transporter activity of NRT1.2/NPF4.6. pYES2-NRT1.2 represents normal NRT1.2/NPF4.6. pYES2-NRT1.2^{S277A}, -NRT1.2^{S277D}, -NRT1.2^{S292A}, -NRT1.2^{S292D}, -NRT1.2^{S277AS292A}, and -NRT1.2^{S277DS292D} represent non-phosphorylated and phosphorylated NRT1.2/NPF4.6 obtained by point mutations at Ser^{277} and Ser^{292} to alanine (A) and aspartate (D), respectively. Empty pYES2 vector was used as a control.

(**B**) ABA import activity in *Xenopus* oocytes expressing NRT1.2/NPF4.6, NRT1.2^{S292A}, NRT1.2^{S292D}, CEPR2^{KD}, or NRT1.2/NPF4.6 plus CEPR2^{KD}. *Xenopus* oocytes injected with water were used as the negative control. Error bars indicate SEM (N = 3). Statistically significant differences were identified between pairs of measurements using Student's *t* test (***$P < 0.001$; ns, not significant).

(**C**) Phenotypes of various seedlings grown on 1/2 MS or 1 μM ABA for 7 d: WT, *nrt1.2-1*, NRT1.2/NPF4.6 complemented (*NRT1.2-COM-1*), NRT1.2/NPF4.6 overexpression (*NRT1.2-OE-1*), NRT1.2^{S292A} and NRT1.2^{S292D} complemented (*NRT1.2^{S292A}-COM* and *NRT1.2^{S292D}-COM*). Error bars indicate SEM (N = 3).

(**D**) Lengths of the primary roots of the seedlings shown in (C). Error bars indicate SEM (N = 3). Bars labeled with different lowercase letters are significantly different from one another ($P < 0.05$; one-way ANOVA).

(**E**) NRT1.2/NPF4.6 protein levels in WT, *nrt1.2-1*, *NRT1.2-COM-1*, *NRT1.2^{S292A}-COM*, and *NRT1.2^{S292D}-COM* seedlings grown on 1/2 MS for 7 d, as determined by western blotting. RbcL was used as the loading control.

(**F**) ABA contents in WT, *nrt1.2-1*, *NRT1.2-COM-1*, *NRT1.2*^{S292A}*-COM*, and *NRT1.2*^{S292D}*-COM* seedlings grown on 1/2 MS for 7 d and treated with ABA for 6 h, as determined by HPLC. Error bars indicate SEM (N = 3). Bars labeled with different lowercase letters are significantly different from one another ($P < 0.05$; one-way ANOVA).

Figure 5. Group XIV ubiquitin-conjugating enzymes UBC32, UBC33, and UBC34 interact with NRT1.2/NPF4.6 and mediate its degradation.

(A) Cell-free degradation of the NRT1.2^{loop}-GST protein in soluble protein extracts from 7-day-old WT seedlings grown on 1/2 MS medium with or without 50 μM MG132 (an inhibitor of the 26S proteasome degradation pathway), 50 μM E64d (an inhibitor of the vacuolar degradation pathway), or both compounds for 0, 0.5, 1, and 2 h. NRT1.2^{loop}-GST protein levels were quantified by western blotting with the anti-GST antibody (indicated by red arrows). RbcL was used as the loading control.

(B) Normalized plot of NRT1.2/NPF4.6 contents based on the band intensities shown in (A). Error bars indicate SEM (N = 3).

(C) MbSUS assays showing that UBC32, UBC33, and UBC34 interact with the NRT1.2/NPF4.6 N-terminal (NRT1.2^{N}, aa 1-231), loop region (NRT1.2^{M}, aa 232-346), and the C terminus of NRT1.2/NPF4.6 (NRT1.2^{C}, aa 347-585). NubWT and NubG were used as positive and negative controls, respectively.

(D) Pull-down assays using purified GST, NRT1.2^{loop}-GST, UBC32$^{\Delta TM}$-His, UBC33$^{\Delta TM}$-His, and UBC34$^{\Delta TM}$-His expressed in *E.coli*. $^{\Delta TM}$ indicates the deletion of the transmembrane regions of UBC32, UBC33, and UBC34.

(**E**) Bimolecular fluorescence complementation (BiFC) assay showing the interaction between UBC32, UBC33, UBC34 and NRT1.2/NPF4.6 in *Nicotiana benthamiana*. ER-Tracker, endoplasmic reticulum dye marker.

(F) In vitro assays of UBC32$^{\Delta TM}$-His, UBC33$^{\Delta TM}$-His, and UBC34$^{\Delta TM}$-His purified from *E.coli* to test for self-ubiquitination. Note that constructs with point mutations (UBC32$^{C93S\Delta TM}$-His, UBC33$^{C87S\Delta TM}$-His, and UBC34$^{C87S\Delta TM}$-His) did not self-ubiquitinate.

(G) Semi-*in vivo* ubiquitination assay using *NRT1.2-OE-1/ubc323334* and UBC32$^{\Delta TM}$-His, UBC33$^{\Delta TM}$-His, and UBC34$^{\Delta TM}$-His (purified from E.coli) to test whether NRT1.2/NPF4.6 is ubiquitinated UBC32, UBC33, and UBC34.

Figure 6. NRT1.2/NPF4.6 is epistatically and negatively regulated by UBC32, UBC33, and UBC34.

(A) Germination phenotypes of WT, *nrt1.2*-1, *ubc323334*, *NRT1.2-OE-1*, *NRT1.2-OE-1/ubc323334*, and *nrt1.2-1ubc323334* plants grown on 1/2 MS with or without 1 μM ABA for 10 d.

(B) Germination rates of the plants shown in (A). Upper panel shows rates on 1/2 MS, and lower panel shows rates on 1 μM ABA. Error bars indicate SEM (N = 3).

(C) Phenotypes of seedlings with the indicated genotypes grown for 7 d on 1/2 MS with or without 1 μM ABA.

(D) Lengths of the primary roots of the seedlings shown in (C). Error bars indicate SEM (N = 3). Bars labeled with

different lowercase letters are significantly different from one another ($P < 0.05$; one-way ANOVA).

(E) NRT1.2/NPF4.6 protein levels in WT and *ubc323334* seedlings grown on 1/2 MS for 7 d before treatment with or without 0.1 mM ABA for 6 h. Protein levels were measured by western blotting. RbcL was used as the loading control.

(F) Normalized plot of the NRT1.2/NPF4.6 degradation shown in (E), based on band intensities. Error bars indicate SEM (N = 3).

Figure 7. Phosphorylation and ubiquitination of NRT1.2/NPF4.6 regulate ABA influx and plant growth in *Arabidopsis.*

Under normal conditions, CEPR2 phosphorylates NRT1.2/NPF4.6 and PYLs at the plasma membrane. The phosphorylated NRT1.2/NPF4.6 and PYLs are translocated to the ER, where they are ubiquitinated by UBC32/33/34. Finally, the ubiquitinated NRT1.2/NPF4.6 and PYLs are degraded by the 26S proteasome and vacuolar degradation pathways. In this scenario, seed germination and primary root growth proceed normally. However, ABA stabilizes NRT1.2/NPF4.6 and PYLs and inhibits their phosphorylation by CEPR2, stimulating NRT1.2/NPF4.6 to import ABA into the cells. Within the cell, ABA is bound by PYLs, triggering the ABA response, which inhibits seed germination and primary root growth.

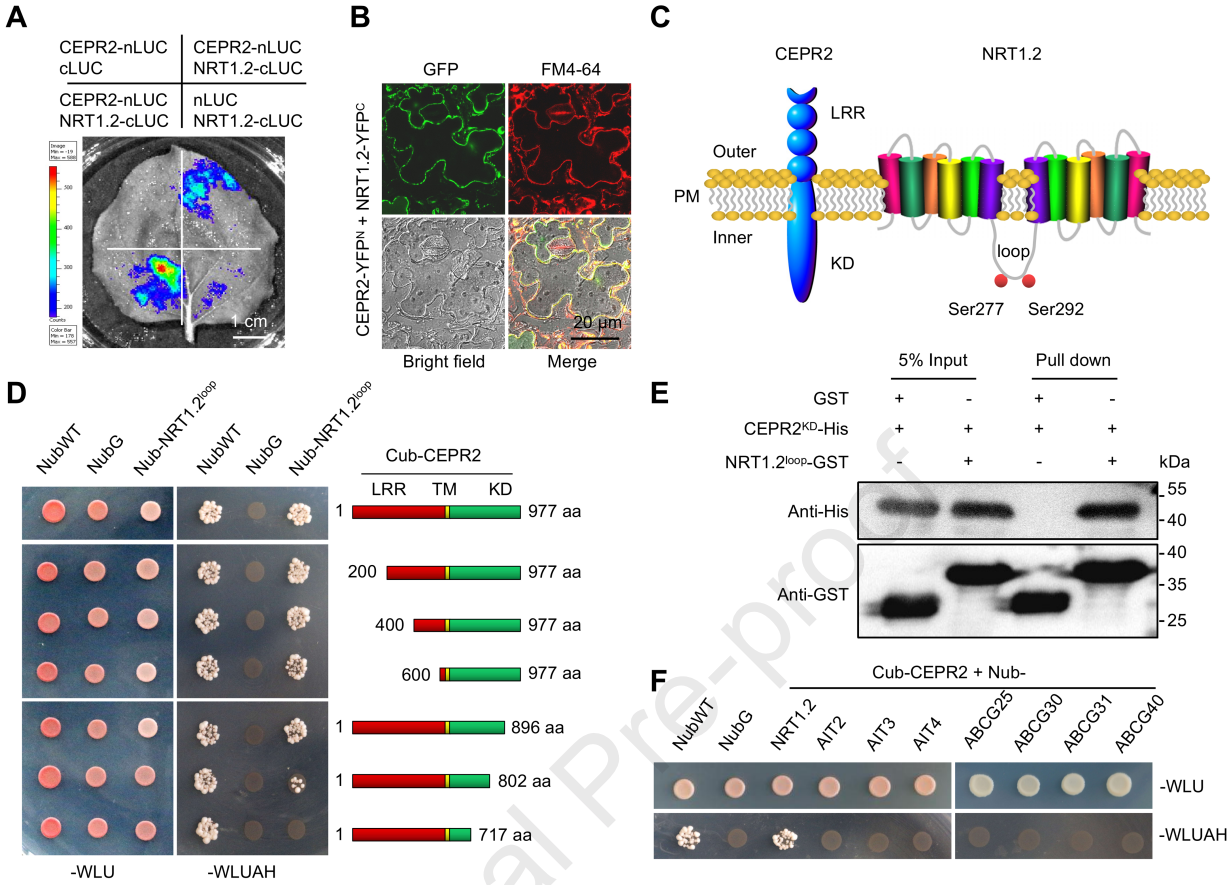

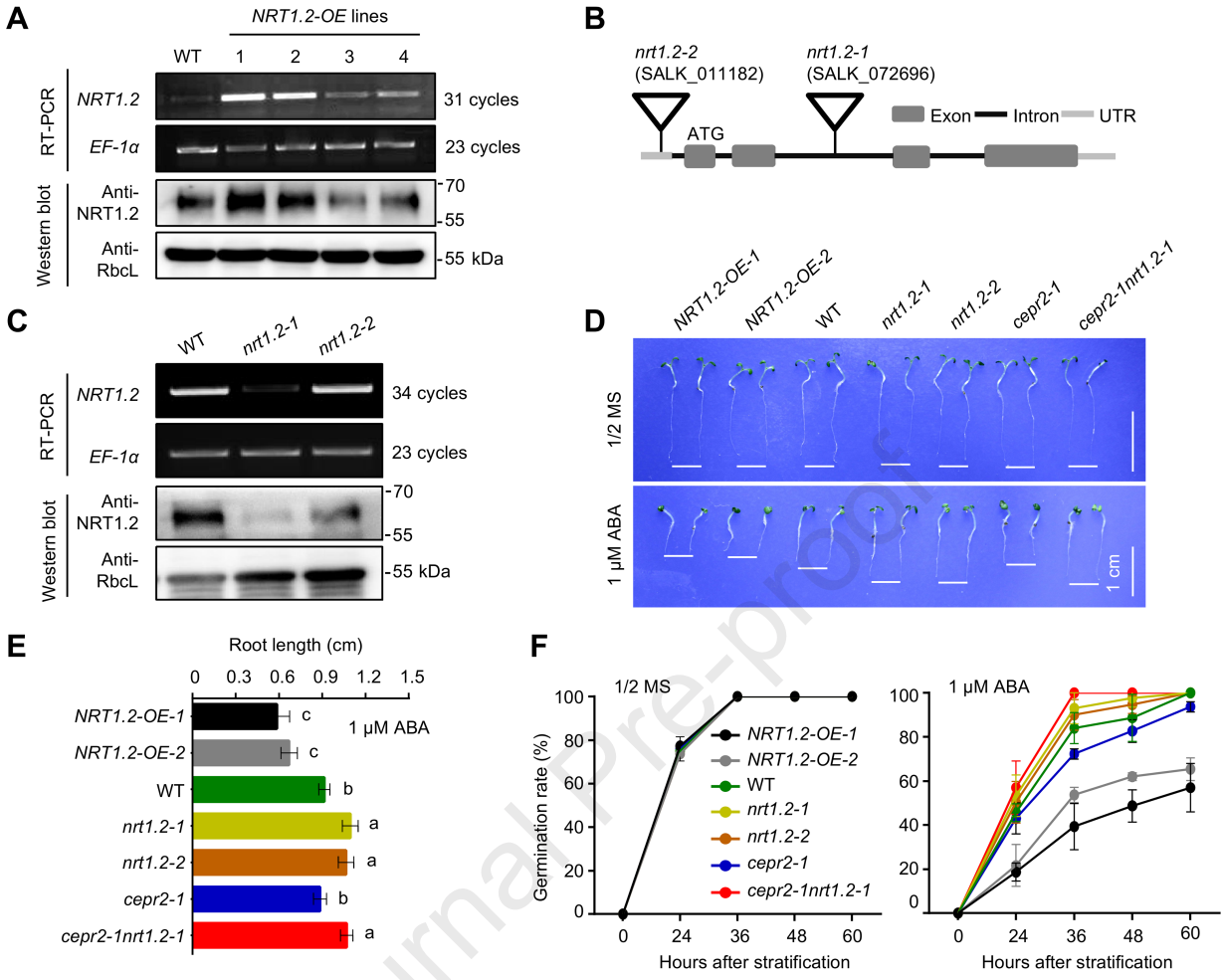

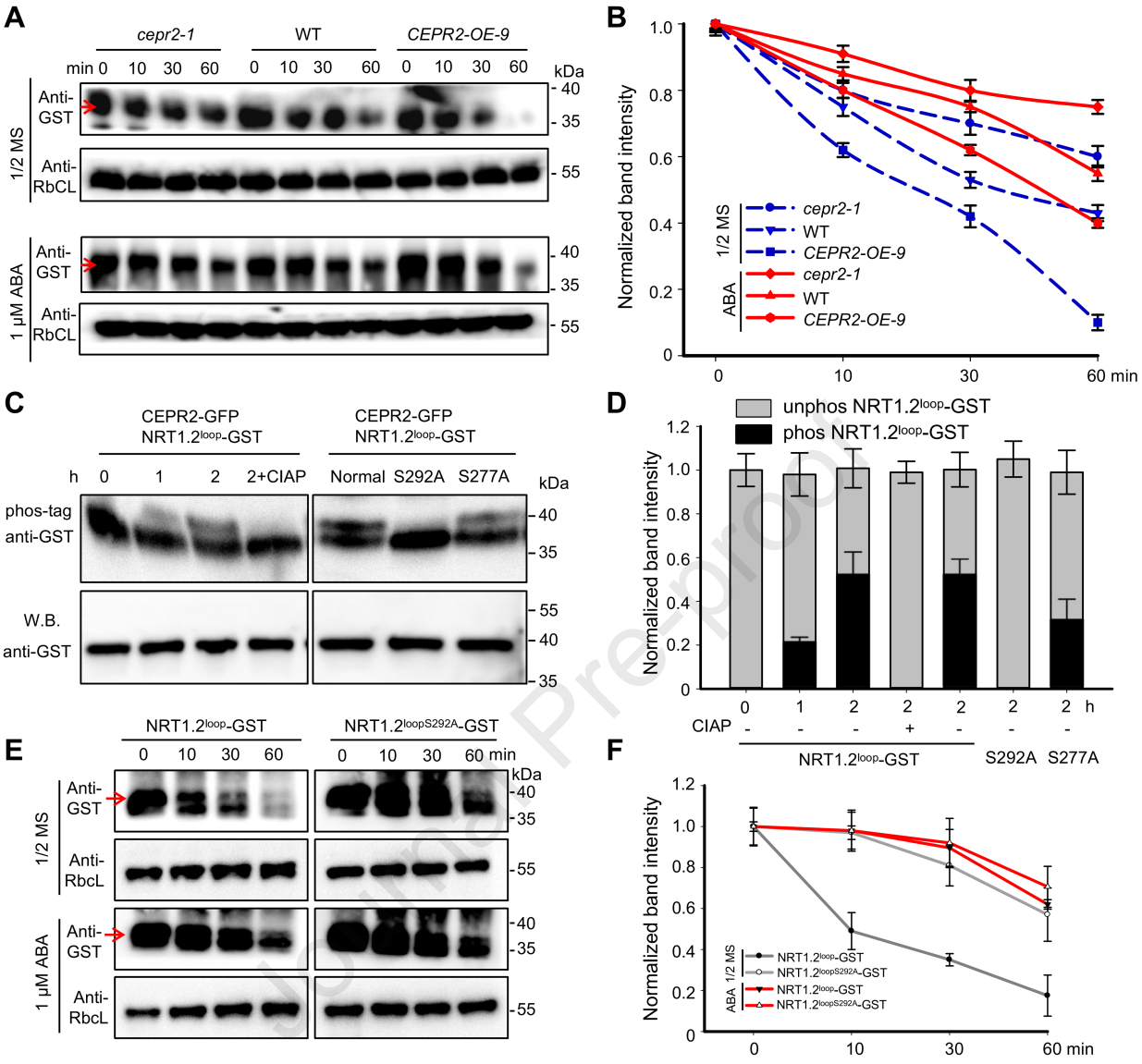
A
cepr2-1
WT
CEPR2-OE-9
min 0 10 30 60 0 10 30 60 0 10 30 60
kDa
1/2 MS
Anti-GST
Anti-RbCL
1 μM ABA
40
35
55
B
Normalized band intensity
1/2 MS
cepr2-1
WT
CEPR2-OE-9
ABA
cepr2-1
WT
CEPR2-OE-9
0 10 30 60 min
C
CEPR2-GFP
NRT1.2loop-GST
h 0 1 2 2+CIAP
CEPR2-GFP
NRT1.2loop-GST
Normal S292A S277A
kDa
phos-tag
anti-GST
W.B.
anti-GST
D
unphos NRT1.2loop-GST
phos NRT1.2loop-GST
Normalized band intensity
0 1 2 2 2 2 2 h
CIAP - - - + - - -
NRT1.2loop-GST
S292A S277A
E
NRT1.2loop-GST
NRT1.2loopS292A-GST
0 10 30 60 0 10 30 60 min
kDa
1/2 MS
Anti-GST
Anti-RbcL
1 μM ABA
F
Normalized band intensity
NRT1.2loop-GST
NRT1.2loopS292A-GST
NRT1.2loop-GST
NRT1.2loopS292A-GST
ABA 1/2 MS
0 10 30 60 min

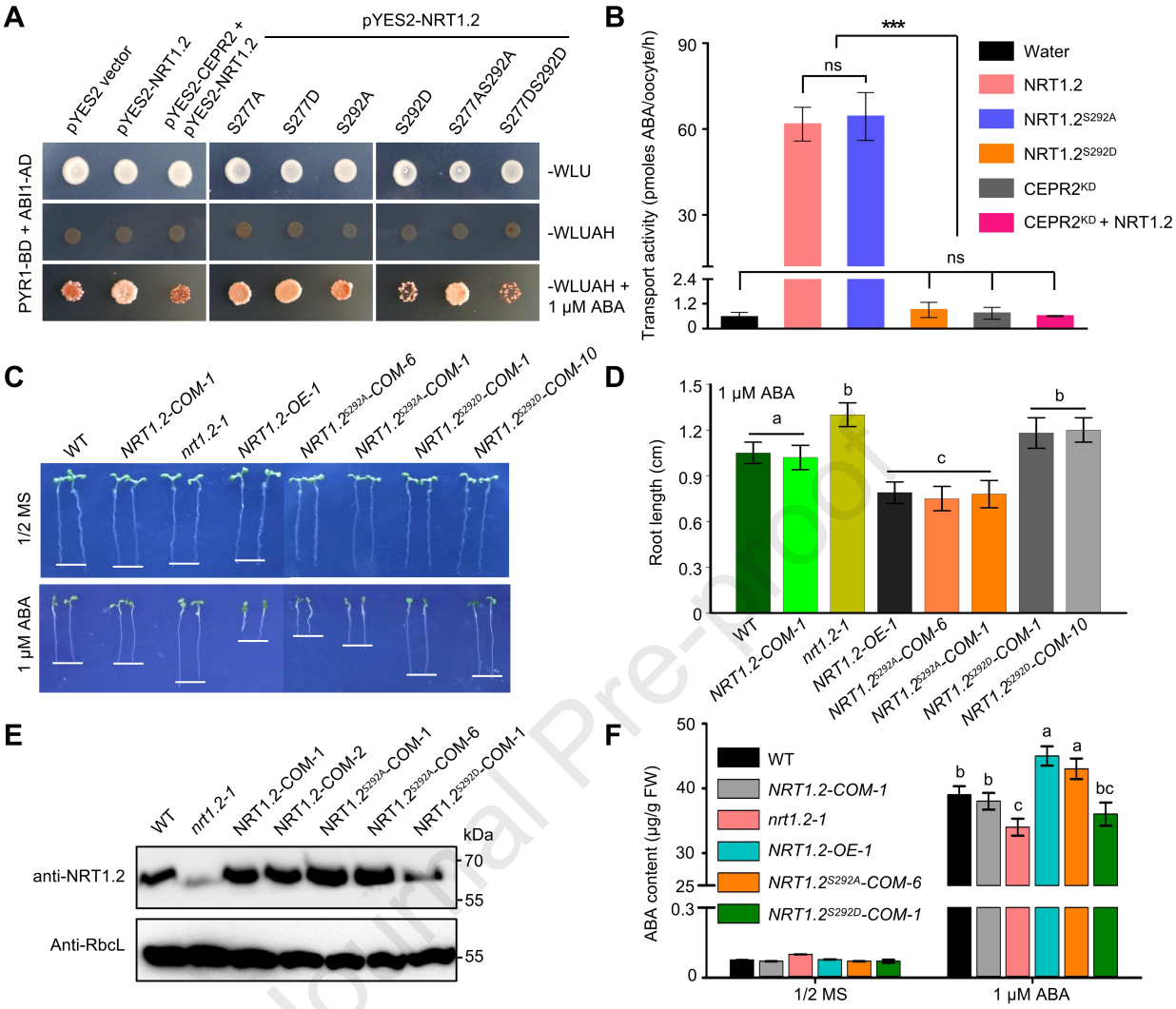

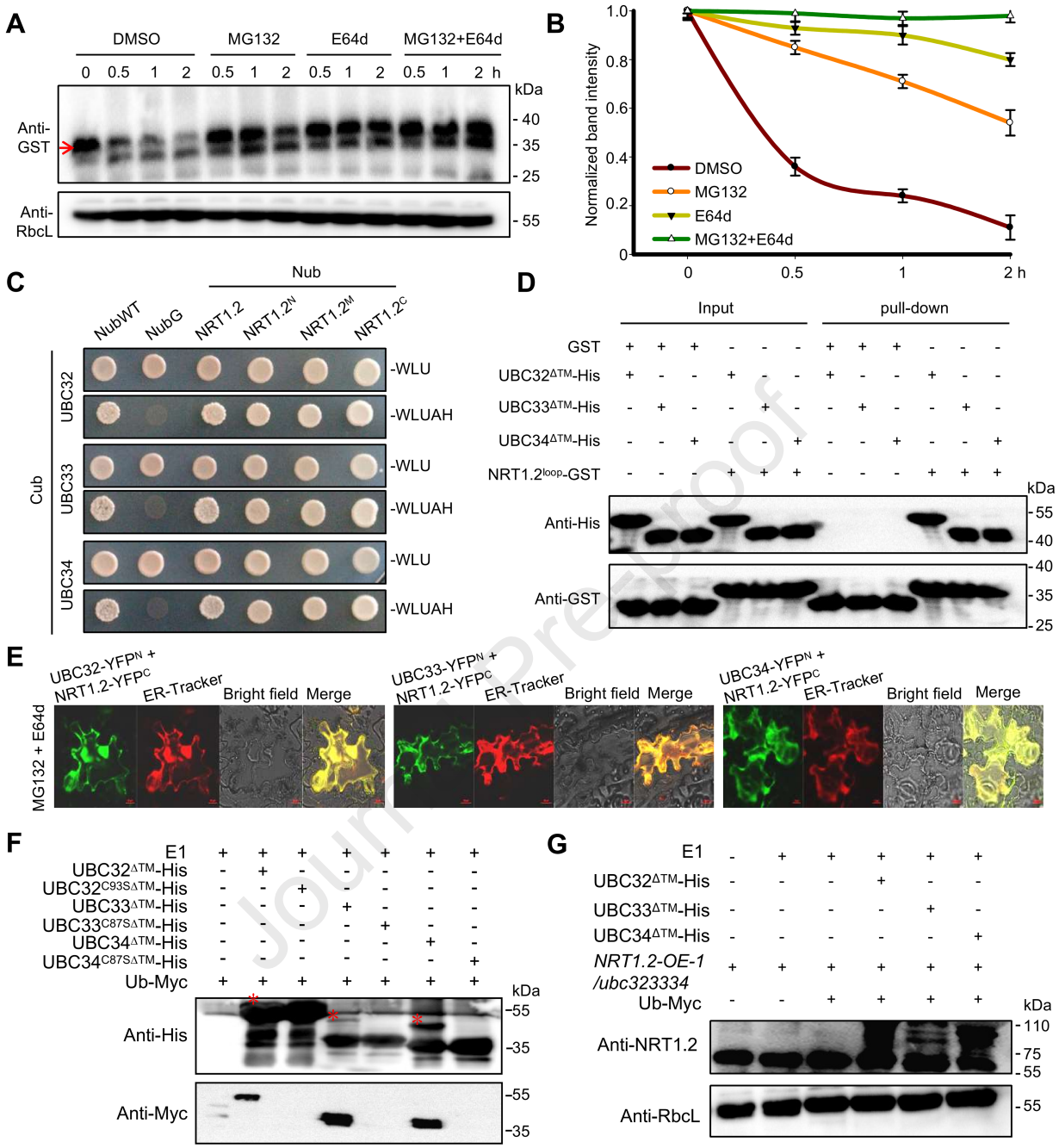
A
DMSO
MG132
E64d
MG132+E64d
0 0.5 1 2 0.5 1 2 0.5 1 2 0.5 1 2 h
kDa
Anti-GST
Anti-RbcL
40
35
25
55
B
Normalized band intensity
1.0
0.8
0.6
0.4
0.2
0
DMSO
MG132
E64d
MG132+E64d
0
0.5
1
2 h
C
Nub
NubWT
NubG
NRT1.2
NRT1.2N
NRT1.2M
NRT1.2C
Cub
UBC32
UBC33
UBC34
-WLU
-WLUAH
D
Input
pull-down
GST
UBC32ΔTM-His
UBC33ΔTM-His
UBC34ΔTM-His
NRT1.2loop-GST
kDa
Anti-His
Anti-GST
55
40
35
25
E
UBC32-YFPN + NRT1.2-YFPC
UBC33-YFPN + NRT1.2-YFPC
UBC34-YFPN + NRT1.2-YFPC
ER-Tracker
Bright field
Merge
MG132 + E64d
F
E1
UBC32ΔTM-His
UBC32C93SΔTM-His
UBC33ΔTM-His
UBC33C87SΔTM-His
UBC34ΔTM-His
UBC34C87SΔTM-His
Ub-Myc
kDa
Anti-His
Anti-Myc
55
35
G
E1
UBC32ΔTM-His
UBC33ΔTM-His
UBC34ΔTM-His
NRT1.2-OE-1 /ubc323334
Ub-Myc
kDa
Anti-NRT1.2
Anti-RbcL
110
75
55